

PACS numbers: 42.55.Rz; 42.60.Fc; 61.48.De
DOI: 10.1070/QE2012v042n08ABEH014775

Mode-locking of solid-state lasers by single-walled carbon-nanotube based saturable absorbers*

F. Rotermund, W.B. Cho, S.Y. Choi, I.H. Baek, J.H. Yim, S. Lee, A. Schmidt, G. Steinmeyer, U. Griebner, D.-I. Yeom, K. Kim, V. Petrov

Abstract. **Universal use of single-walled carbon-nanotube based saturable absorber devices for mode-locking of bulk solid-state lasers between 0.8 and 2 μm is discussed. The advantages in comparison to semiconductor saturable absorbers are emphasised. We briefly describe the manufacturing process and the essential optical properties, and review experimental results obtained with various types of femtosecond and picosecond solid-state lasers in the steady-state regime. We also demonstrate that a single hybrid saturable absorber used in transmission can be used to mode-lock four different types of lasers operating between 1 and 2 μm.**

Keywords: *single-walled carbon nanotubes, passive mode-locking, solid-state lasers.*

1. Introduction

Recent developments indicate that single-walled carbon nanotubes (SWCNTs) can be successfully employed as ultrafast saturable absorbers (SAs) for mode-locking solid-state lasers, representing a real alternative to the widely spread semiconductor saturable absorber mirrors (SESAMs). However, while SESAMs exhibit a spectrally narrowband nonlinearity, require sophisticated manufacturing processes and mandate controlled defect implantation to warrant ultrafast response times, SWCNT-SAs are characterised by broadband absorption with large third-order nonlinearity and can be fabricated by relatively simple methods. The absorption band of SWCNT-SAs can be controlled by varying the nanotube diameter and chirality and, depending on the electronic transitions of semiconducting nanotubes, covers the near-IR spectral range from ~0.8 up to ~2.0 μm. In addition, such SAs can be designed in transmission type for extended spectral coverage.

The first demonstration of passive mode-locking with a SWCNT-SA was realised with Er-doped fibre lasers [1] and most of the subsequent efforts were restricted to such fibre lasers because their single-pass gain can easily tolerate relatively high nonsaturable insertion losses, see e.g. [2, 3]. For application of SWCNT-SAs in bulk solid-state lasers it is necessary to reduce the nonsaturable losses to the lowest level possible [3]. The first demonstration of bulk solid-state laser mode-locking was based on the same Er^{3+} transition in glass at 1.57 μm [4]. This stimulated a lot of activities with various solid-state lasers based on rare-earth and transition metal dopants exhibiting very different spectroscopic characteristics such as emission cross sections, fluorescence linewidths and lifetimes. In this overview, the results obtained in the picosecond and femtosecond continuous-wave (cw) mode-locked regimes using transmission and reflection type SWCNT-SAs in various bulk solid-state lasers operating between 0.8 and 2 μm will be reviewed. These include femtosecond $Ti:Al_2O_3$ (sapphire) lasers near 0.8 μm, femtosecond Yb- and femtosecond/picosecond Nd-lasers in the 1 μm spectral range, femtosecond $Cr:Mg_2SiO_4$ (forsterite) lasers near 1.25 μm, picosecond Nd-lasers near 1.34 μm, femtosecond $Cr:Y_3Al_5O_{12}$ (YAG) lasers near 1.5 μm and Er-lasers near 1.6 μm, and picosecond Tm-lasers near 1.95 μm.

2. Fabrication and properties of SWCNT-SAs

Depending on their chirality, SWCNTs possess metallic or semiconducting properties. Semiconducting SWCNTs exhibit pronounced optical nonlinearity. They are chemically stable and resistant to optical damage. Since the absorption resonance of the electronic interband transition depends on the diameter and chirality, natural mixtures of SWCNTs automatically provide broadband absorption in the near-IR from ~0.8 to ~2 μm (Fig. 1). Therefore, the dispersion of natural SWCNT mixtures covers the spectral extension of several rare-earth (Yb^{3+}, Nd^{3+}, Er^{3+}, Tm^{3+}) and transition metal (Ti^{3+}, Cr^{4+}) ion doped solid-state laser materials.

As with any SA, residual losses in the fully saturated SWCNTs have to be as low as possible, in any case small compared to the single pass laser gain. This condition is easy to fulfil in fibre lasers; however, using SWCNTs for mode-locking of bulk solid-state lasers with their few-percent output coupling is far more challenging. Unfortunately, regardless of the preparation technology used, nonsaturable losses are always present. First of all, SWCNTs will always exhibit scattering. If they are considered as completely isolated cylindrical objects, Rayleigh scattering with a cross section $\sigma_{cyl}(\lambda) \propto r^4\lambda^{-3}$ will prevail, with nanotube radius r and wavelength λ. Depending on preparation of the SWCNT dispersion and the coating process, more or less pronounced bundling and curl-

*Reported at the XIX International Conference on Advanced Laser Technologies, Bulgaria, Golden Sands, September 2011.

F. Rotermund, W. B. Cho, S. Y. Choi, I. H. Baek, J. H. Yim, S. Lee, D.-I. Yeom, K. Kim Division of Energy Systems Research, Ajou University, 443-749 Suwon, Republic of Korea;
A. Schmidt, G. Steinmeyer, U. Griebner, V. Petrov Max Born Institute for Nonlinear Optics and Short Pulse Spectroscopy, 2A Max-Born-Str., 12489 Berlin, Germany; e-mail: petrov@mbi-berlin.de

Received 8 November 2011
Kvantovaya Elektronika **42** (8) 663–670 (2012)
Submitted in English

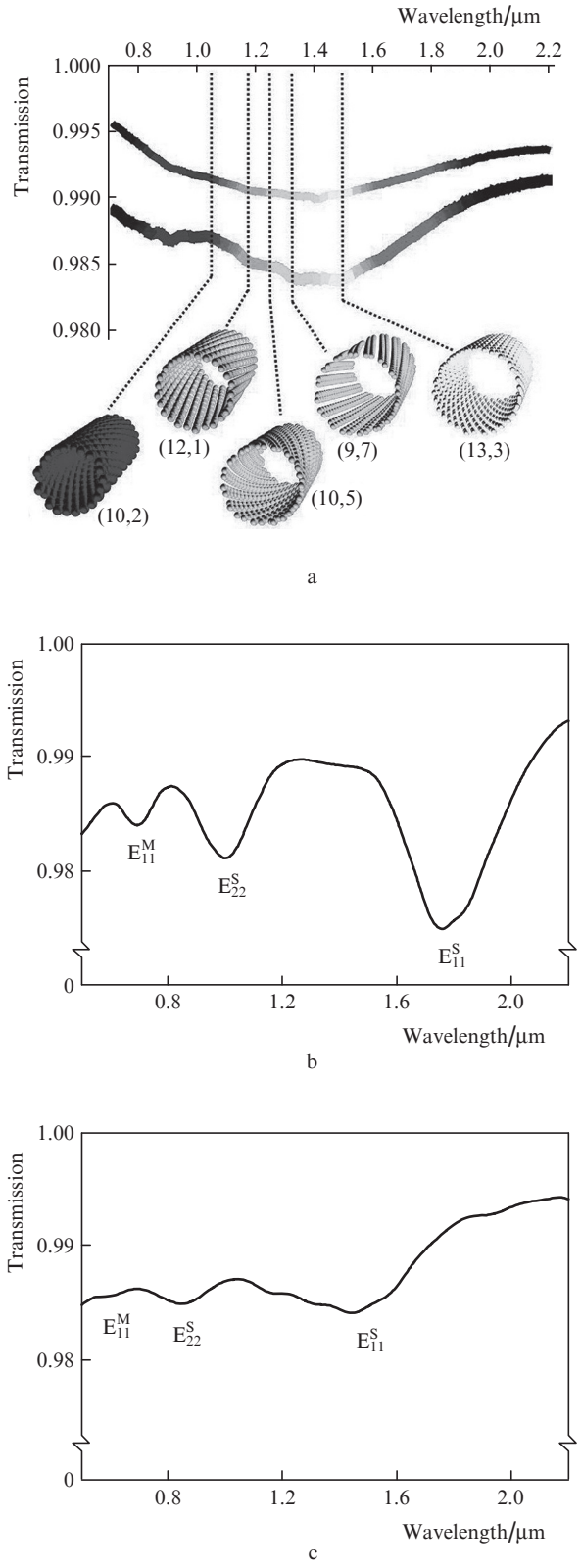

Figure 1. (a) Transmission spectra of two transmissive HiPCO SWCNT saturable absorbers with different optical densities. Spectral location of the absorption caused by nanotube species with chiral vector (n,m) identified from Raman spectroscopic measurements are indicated by dashed lines. (b) Typical absorption spectra of arc-discharge SWCNT (diameter 1.2–1.4 nm) and (c) HiPCO SWCNT (diameter 0.8–1.2 nm) saturable absorbers with indicated transitions (S – semiconductor, M – metallic character).

ing may occur, causing nanotubes to interweave, eventually forming macroscopic ball-like objects with much less favourable scattering properties $\sigma(\lambda) \propto r^6\lambda^{-4}$ that may ultimately merge into Mie scattering. On the other hand, however, bundling may also serve to increase the number of tube-to-tube interactions to some extent. This effect may act beneficially in accelerating absorber relaxation but has a much less pronounced effect on scattering than the curl. Control of the statistical distribution of nanotubes is therefore the key to balancing nonsaturable absorber losses and accelerated relaxation. Finally, SWCNTs as SA devices may also exhibit Bragg losses for reflective design or Fresnel losses when used in transmission.

Initial studies of SWCNT based SAs for bulk laser mode-locking revealed nonsaturable losses around 1% with a ratio of useful (saturable) to unwanted (nonsaturable) losses, not exceeding 1:2. In some cases, also relatively high saturation fluences, $F_{sat} > 50$ μJ cm^{-2}, were observed [5], which may cause Q-switched mode-locking and optical damage in bulk solid-state laser cavities. Therefore, application of SWCNT SAs for bulk solid-state laser mode-locking has been quite limited so far. All such experimental demonstrations will be reviewed in the next section. In most of our own mode-locking experiments with SWCNT based SAs, arc-discharge grown SWCNTs (arc-discharge SWCNTs) or SWCNTs synthesised by high-pressure CO decomposition (HiPCO) method were employed. In comparison to HiPCO grown SWCNTs, arc-discharge SWCNTs are longer and also exhibit a stronger tendency to curl up and form ball-like aggregates.

In our experiments, arc-discharge SWCNTs (Iljin Nanotech) or HiPCO SWCNTs (Unidym) were used for manufacturing SAs without further purification since thermogravimetric analysis indicated purities as high as 90%. The SWCNTs were first dried in vacuum and then dispersed in dichlorobenzene (DCB) via ultrasonic agitation with different concentrations between 0.1 and 0.25 mg mL^{-1}. Subsequently, poly(*m*-phenylenevinylene-2,5-dioctoxy-*p*-phenylenevinylene) (PmPV) was added during the ultrasonic process to enhance solubility of SWCNTs. Details on the ultrasonication procedure for arc-discharge SWCNTs can be found in [6]. Applying a similar procedure to HiPCO SWCNTs, the bundling of the relatively long SWCNTs was still too strong and the resulting scattering loss quite large. Therefore, a multi-step ultrasonication process was used to achieve de-bundling and breaking longer nanotubes to shorter lengths, details can be found in [7]. A separately prepared polymethyl methacrylate (PMMA) solution was finally mixed with the SWCNT dispersion at an identical volume ratio, followed again by ultrasonication and stirring. The SWCNT/PMMA films were spin-coated onto quartz substrates in a single-step process using different rotation speeds, controlling the transmission by varying the thickness of the coated film and (mainly) the SWCNT concentration. Alternatively, identical films could be directly deposited on commercial highly reflecting dielectric mirrors for manufacturing reflective SA devices. The coated samples were finally baked at 150 °C. The resulting thickness of the SWCNT/PMMA layer was typically in the 200–300 nm range. The deposited absorber layer was uniform across the whole substrate. No antireflection coatings were deposited on the SWCNT/PMMA-coated surfaces.

Figure 1a shows typical transmission spectra of two transmission type SAs fabricated with different HiPCO SWCNT concentrations. The ultrabroad absorption band in the 1 to 1.8 μm range is mainly attributed to an overlap of the first

interband transitions (E_{11}) in semiconducting SWCNTs of different diameters and chiralities, with intertube interaction causing further broadening. Raman spectroscopy of SWCNTs and SWCNT/PMMA composite films provides information on the diameter and chirality of the distributed SWCNTs. These measurements indicated the presence of SWCNTs with five clearly visible chiralities whose resonant absorption is located in the spectral range between 1 and 1.5 μm (Fig. 1a). Further SWCNT species might be present, contributing to the broadband absorption, although they did not show up in the Raman spectra [7].

The E_{22} interband transition of HiPCO SWCNTs can be used on the other hand for the 800 nm spectral range (Ti:sapphire lasers, Fig. 1b). As can be also seen from Fig. 1b, the absorption bands in arc-discharge SWCNT SAs are spectrally shifted to longer wavelengths, the E_{22} interband transition is then applicable to 1-μm (Nd-, and Yb-doped) lasers and the E_{11} interband transition to 2-μm (Tm-doped) lasers. This wavelength shift is due to different distribution of the SWCNTs with respect to chirality and diameter.

Scanning electron microscopy (SEM) images of the SAs indicated that HiPCO SWCNTs are mostly stretched out [7]. Low scattering losses can be expected in this case since SWCNTs do not appear to be extremely curled or interweaved into one another as often observed in earlier studies. High-resolution transmission electron microscopy (TEM) images revealed small bundles of different SWCNTs, with bundle diameters ranging to a maximum of about 20 nm [7]. This bundle topology might be beneficial as it gives rise to strong tube-to-tube coupling while only moderately increasing Rayleigh scattering at the same time.

The nonlinear optical characteristics of the SWCNT-based SAs can be studied by nonlinear transmission and pump-probe measurements in the 0.8–2 μm wavelength range [6, 7]. The nonlinear transmission experiments indicated nonsaturable absorption of typically ~1% (Fig. 2) but in some cases values down to < 0.5% have been observed. The modulation depth is in the 0.3%–0.4% range (Fig. 2). In the best cases, nonsaturable and saturable losses are comparable. The low losses in HiPCO SWCNTs are related to the relatively weak curl tendency and their favourable habit to unweave and bundle during the ultrasonication process [7]. Another beneficial factor might be the shorter length of HiPCO nanotubes as a result of the multi-step ultrasonication process. All these effects together suppress the formation of ball-like objects or their precursors.

SWCNTs also intrinsically ensure single-picosecond relaxation times of the saturable absorption. The pump-probe curves can be deconvolved using a bi-exponential kernel function, physically justified by the presence of fast intraband carrier relaxation in non-resonantly excited nanotubes and a slower interband carrier recombination in resonantly excited nanotubes (Fig. 3). Deconvolution of data obtained with transmission type HiPCO SWCNT SAs yields fast relaxation time constants increasing from about 70 fs at 1060 nm to 300 fs at 1.55 μm [7]. This trend is caused by the dominant fast intraband contribution, which decelerates in the vicinity of the E_{11} transitions of the largest nanotubes in the mixture. The slow component, however, is clearly discernible, giving rise to a small pedestal at positive delays. The latter is missing at 1.92 μm, and only a faint fast response can be seen. Clearly, a SA based on HiPCO SWCNTs is not useful for operation at this particular wavelength, where arc-discharge SWCNTs are more suitable (Fig. 1b). The markedly different behaviour observed at 1.92 μm further confirms the assignments in the two-time-constant model as no direct electronic transition may occur anymore below the electronic excitation energy of the largest nanotubes in the mixture. The measured 70–300 fs recovery times of the E_{11} transition are shorter than previously reported values for the E_{22} transition in SWCNT absorbers based on the arc-discharge [6] or laser ablation [5] methods. This can be attributed to the nanotube bundling, in particular to their pronounced tendency to curl together. The slow relaxation constant is in the 1–2 ps range for both types, arc-discharge and HiPCO SWCNTs. Finally, the saturation fluences of about 10 μJ cm^{-2} of HiPCO SWCNT absorbers (see Fig. 2), also appear to be systematically higher than typical values measured for arc-discharge SWCNTs [6], which are on the order of 5 μJ cm^{-2}. However, the values are in general not so different and in any case sufficiently low to avoid *Q*-switching instabilities. As the elementary SWCNTs manufactured by either method are ultimately similar, this systematic difference can only stem from different size distributions and chiralities or microscopic orders.

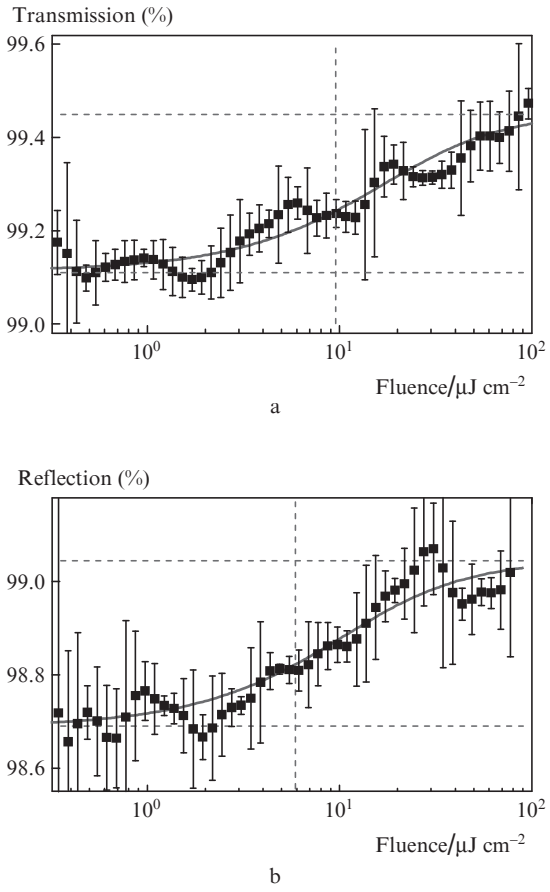

Figure 2. Nonlinear transmission and reflection measurements of a HiPCO SWCNT based saturable absorber of (a) transmission (modulation depth, 0.37%; nonsaturable loss, 0.95%) and (b) reflection (modulation depth, 0.34%; nonsaturable loss, 1.3%) type at 1.3 μm, near the centre of the absorption band for a pulse duration of 100 fs. Error bars indicate standard deviations. Thick curves represent fits to a model function, with the resulting values of saturated and nonsaturated transmission/reflection indicated by horizontal dashed lines and the saturation fluence F_{sat} = 9.5 (a) and 6.0 (b) μJ cm^{-2} indicated by the vertical dashed line.

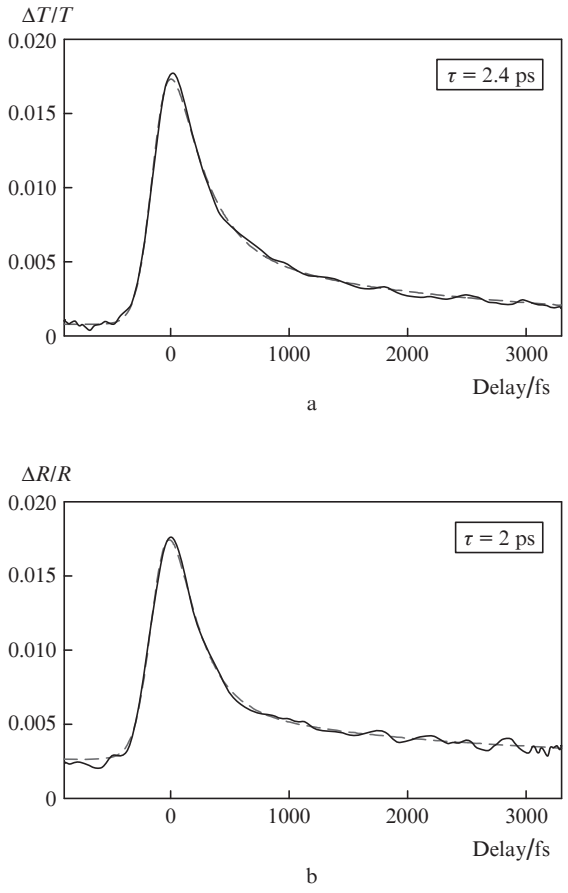

Figure 3. Pump-probe measurements of a HiPCO SWCNT based saturable absorber of (a) transmission and (b) reflection at 1.3 μm with 100 fs pulses. Dashed curves represent fits to the experimental data (solid curves). The indicated time constants refer to the slow relaxation process.

At 800 nm (E_{22} transition in HiPCO SWCNTs) the relaxation constants were similar but the modulation depth was smaller (0.15%) while the saturation fluence was ~30 μJ cm^{-2}. Furthermore, above 200 μJ cm^{-2}, two-photon absorption (TPA) comes into play at 800 nm.

In general, the characteristics of SWCNT-based SAs are very similar to those of SESAMs (in the restricted wavelength ranges where such devices are commercially available) with the exception of the saturation fluence which is higher in SESAMs by roughly one order of magnitude. This means that stable mode-locked operation in the steady state cw regime can be expected in a broader power range with SWCNT-based SAs, also at low powers approaching the threshold. Besides the simpler and cheaper technology for their manufacturing, SAs based on SWCNTs are expected to have superior damage resistivity compared to SESAMS which has been confirmed in few cases at least with respect to commercially available SESAMs.

3. Bulk solid-state laser mode-locking in the steady-state cw regime

Here we will review the results obtained so far with steady-state mode-locked solid-state lasers because the regime in pulsed systems (e.g. flash-lamp pumped or simultaneous *Q*-switched) is very different. Table 1 summarises the essential laser parameters achieved with different laser materials and different types of SWCNT-based SAs.

As already mentioned, the first successfully mode-locked bulk laser with SWCNT SA was Er : glass [4], generating 68-fs pulses at 1570 nm under diode-pumping at 980 nm. The reflection type SA was used as an end mirror and no dispersion compensation was necessary at this wavelength. The second Er : glass laser mode-locked by reflective SWCNT SA [5] had a similar design, diode-pumped at 976 nm. Without dispersion compensation, 1.8-ps pulses were generated while incorporating Gires–Tournois interferometer mirrors resulted in higher average output power, however, at the expense of longer pulse duration in comparison to [4].

In the same work [4] it was only mentioned that a Nd : glass laser also produced femtosecond pulses mode-locked by a SWCNT SA. More recently Nd : silicate glass laser mode-locked by reflective type SWCNT SA generated pulses as short as 99 fs [17], pumped by a low power (200 mW) 805-nm laser diode. Dispersion compensation by two intracavity prisms was employed in this case. The overall performance was compared with SESAM and the mode-locked laser characteristics were quite similar. A similar comparison with Nd : phosphate glass, in general yielding longer pulse durations, was performed in [13] using the same pump source and SWCNT SA in single and two-prism cavity configurations.

The first narrow-band, crystalline Nd-laser mode locked by a SWCNT SA was Nd : BaY_2F_8 [12]. Using the same reflective SA as in [13, 17], picosecond pulse generation was achieved from a cavity without dispersion compensation. The fact that Nd : YAG or Nd : YVO_4 did not mode-lock under identical conditions was explained by strong gain saturation. In order to suppress this effect a higher ratio of saturable to nonsaturable losses would be required. Picosecond mode-locking of ceramic Nd : YAG has been eventually achieved, employing purified semiconducting SWCNTs of chirality (7.5) in a reflective type SA employed as an end mirror in a cavity without dispersion compensation [16]. From *z*-scan measurements these authors reported saturable and nonsaturable losses roughly 10 times higher and saturation fluence roughly 10 times lower at 1040 nm (see previous section). The mixed (disordered) vanadate crystal Nd : $Lu_{0.15}Y_{0.85}VO_4$, exhibiting broader fluorescence bandwidth and smaller emission cross section, was also successfully mode-locked by a transmission type SWCNT SA [15] in a cavity without dispersion compensation. However, this type of SA exhibited small modulation depth but high nonsaturable losses and high saturation fluence, cw mode-locking occurred only above the region of *Q*-switched mode-locking, and the obtained pulse duration (19 ps) is too long with respect to the available gain bandwidth. The highest average power (3.63 W) ever achieved with a picosecond bulk solid-state laser mode-locked by SWCNT SA, was obtained with Nd : $GdVO_4$ [14]. The transmission type SA was manufactured without polymer for higher damage resistivity. It exhibited roughly 10 times higher saturable absorption and saturation fluence (compare with the previous section); however, the nonsaturable losses were about 5 times larger than the saturable losses.

SWCNT SAs were recently applied also at 1.34 μm, to mode-lock a diode-pumped Nd : YVO_4 laser operating on the $^4F_{3/2} \rightarrow {}^4I_{13/2}$ transition [20]. Picosecond pulses were generated from a cavity optimised for large fundamental mode volume. With a transmission type SA based on HiPCO SWCNTs the

Table 1. SWCNT-SA CW mode-locked bulk solid-state lasers.

Material	Wavelength/nm	Pulse duration/fs	Repetition rate/MHz	Power/mW	SWCNT type (T – transmission, R – reflection)	Reference
Ti:Al_2O_3	810	600	110	45	HiPCO (R)	[8]
	800	62	99.4	600	HiPCO (T)	[9]
Yb:$KY(WO_4)_2$	1038	140	88	32	Arc-discharge (T)	[10]
	1049	83	84	24	Arc-discharge (R)	
Yb:$KLu(WO_4)_2$	1048	115	89	30	Arc-discharge (T)	[11]
Nd:BaY_2F_8	1049	8500	194	70	Arc-discharge (R)	[12]
Nd:phosphate glass	1054	~200	—	—	CO* (R)	[4]
	1056	160	194	8	Arc-discharge (R)	[13]
Nd:$GdVO_4$	1063	8400	122	3630	Arc-discharge (T)	[14]
Nd:$Lu_{0.15}Y_{0.85}VO_4$	1064	19000	150	902	Arc-discharge (T)	[15]
Nd:$Y_3Al_5O_{12}$ (YAG ceramics)	1064	8300	90	130	CO* (R)	[16]
Nd:silicate glass	1070	99	194	10	Arc-discharge (R)	[17]
Cr:Mg_2SiO_4	1245	120	79	202	HiPCO (T)	[18]
	1250	80	78	295	HiPCO (R)	[19]
Nd:YVO_4	1342	16500	127	800	HiPCO (T)	[20]
Cr:$Y_3Al_5O_{12}$ (YAG)	1495	92	85	110	HiPCO (T)	[21]
Er,Yb:phosphate glass	1570	68	85	~30	Laser ablation (R)	[4]
	1562	261	75	63		[5]
Tm:$KLu(WO_4)_2$	1944	9700	126	240	Arc-discharge (T)	[22]
Yb:$KY(WO_4)_2$	1038	133	87	160		
Cr:Mg_2SiO_4	1242	100	79	230	HiPCO (T)	[7]
Cr:$Y_3Al_5O_{12}$ (YAG)	1495	92	85	110		
Yb:$KLu(WO_4)_2$	1069	84	89	62		
Cr:Mg_2SiO_4	1243	118	79	250	Arc-discharge–HiPCO	[23]
Cr:$Y_3Al_5O_{12}$ (YAG)	1485	113	85	85	(T)	
Tm:$KLu(WO_4)_2$	1942	25400	130	167		

* – CO is the disproportionation reaction (CO decomposition into C and CO_2).

pulse energies achieved in this first experiment compare well with the best results obtained with SESAMs (more or less exotic at this wavelength) mode-locking while the pulse duration (16.5 ps, no dispersion compensation) is substantially shorter.

Yb-doped crystalline lasers, in contrast to their Nd analogues, can provide femtosecond pulse durations near 1-μm employing cavities with intracavity dispersion compensation. Monoclinic double tungstates are hosts that provide one of the broadest emission bandwidths. We successfully mode-locked Yb:$KLu(WO_4)_2$ and Yb:$KY(WO_4)_2$ lasers employing both transmission and reflection type arc-discharge SWCNT SAs in cavities containing a prism pair for dispersion compensation [10, 11]. Sub-100-fs pulse durations were achieved and the results were close to those that could be obtained with SESAMs which are widely used in this wavelength range. Note that such broadband Yb-lasers also can be tuned in wavelength to some extent, still producing femtosecond pulses [10].

Cr^{4+}:forsterite was the first transition metal, widely tunable laser that we tried to mode-lock using transmission type HiPCO SWCNT SA because in this wavelength range (near 1.25 μm) SESAMs are simply absent. Self-starting operation was achieved in the femtosecond regime using an intracavity prism pair for dispersion control [18]. With a reflection type SA used in a similar cavity, 80-fs pulses at 1250 nm were generated with an average power of 295 mW, the highest ever achieved for any femtosecond laser mode-locked by a SWCNT SA [19]. We also successfully mode-locked the related Cr:YAG laser, operating at longer wavelengths near 1.5 μm, using similar transmission type HiPCO SWCNT SA operating on the same semiconducting type E_{11} transition. With intracavity dispersion compensation, stable and self-starting mode-locked operation was achieved. Sub-100-fs transform-limited pulses were generated, tunable in the 1460–1500 nm spectral range [21].

In the extremes of the spectral coverage of SWCNTs (see Fig. 1), we successfully used them for mode-locking of Ti:sapphire lasers at 800 nm and Tm-lasers near 1.95 nm. The E_{22} semiconductor type transition in transmission type HiPCO SWCNT SA was utilised in the case of Ti:sapphire employing an intracavity prism pair for dispersion compensation. It is known that Ti:sapphire lasers self mode-lock (Kerr lens mode-locking, KLM). In contrast to the general belief, however, SWCNT-SA-assisted mode-locking enabled shorter pulse durations and broader spectral bandwidths compared

to pure KLM [9]. Pulses as short as 62 fs were achieved at average power of 600 mW, both values presenting an improvement by more than an order of magnitude in comparison to a previously published report by others [8]. Our femtosecond Ti:sapphire laser was also easily tunable between 780 and 825 nm. Thus, despite of the TPA which is present at high power levels, it can be concluded that low-cost and properly engineered SWCNT-SAs can be successfully used as an alternative to widespread SESAMs also for ultrafast Ti:sapphire lasers.

In the case of $Tm:KLu(WO_4)_2$ we relied on the E_{11} transition in arc-discharge SWCNT SA. The advantage of the double tungstate host in this case is the relatively short Tm lifetime which is beneficial for suppression of *Q*-switching instabilities. Self-starting and stable mode-locking was achieved at 1944 nm with bandwidth-limited pulses of 9.7-ps duration in the absence of intracavity dispersion compensation [22]. Although much shorter pulse durations are supported by the emission bandwidth of $Tm:KLu(WO_4)_2$, it should be emphasised that this initial experiment represents the first demonstration of passive mode-locking of a bulk 2 μm (Tm- or Ho-) solid-state laser.

Transmission type SAs based on SWCNTs offer the unique possibility for universal application in different types of lasers. For experimental verification, we used one and the same HiPCO SWCNT SA to mode-lock three different bulk solid-state lasers on the E_{11} semiconductor type transition, namely $Yb:KY(WO_4)_2$ near 1.04 μm, Cr:forsterite near 1.24 μm, and Cr:YAG near 1.5 μm [7]. In fact, it can be seen from Table 1 that this is the same SA already reported before for Cr:YAG mode-locking [21]. All lasers operated in the femtosecond regime with an intracavity prism pair for dispersion compensation. Autocorrelation measurements indicated pulse durations of 92–133 fs [7]. In all cases, this leads to time-bandwidth products < 0.34, i.e., close to the Fourier limit. We achieved stable mode-locking throughout, as indicated by pedestal-free (> 60 dB) intermode beats. The practical and unconditional absence of *Q*-switching instabilities in all three lasers confirms the very low saturation fluence of this type of SWCNT SA.

Mode-locking of the three bulk femtosecond lasers mentioned above in the spectral range of 1–1.5 μm was self-starting and could be maintained over hours. No signs of degradation were seen after several months of operation at regular atmospheric conditions without forced cooling of the device. This appears quite remarkable, as the SA was driven at intracavity peak intensities close to 10^9 W cm^{-2} and at fluences up to $100F_{sat}$. It should be recalled, however, that nonsaturable losses in SWCNTs are only caused by scattering and therefore cannot induce sample heating. This rather benign nature of nonsaturable losses and the large band-gap of the PMMA host therefore set SWCNT based SAs apart from SESAMs.

Recently we achieved octave-broad bandwidth (~1000 nm) coverage by mixing two differently grown SWCNTs. This hybrid ultra-broadband SA device was employed for mode-locking of Yb-, Cr- and Tm-doped bulk solid-state lasers at wavelengths near 1.07, 1.24, 1.5 and 1.94 μm (preliminary results were reported in [23], see Table 1). For this sample, pump-probe spectroscopy at different wavelengths in the 1–2 μm range revealed similar fast bi-exponential behaviour with the slow component of < 2 ps. The nonlinear transmission measurements of the hybrid type SWCNT SA indicated non-saturable losses of ~1.0% together with typical modulation depths of $< 0.5\%$ and saturation fluence of < 10 μJ cm^{-2}.

$Yb:KLu(WO_4)_2$, Cr:forsterite, Cr:YAG and $Tm:KLu(WO_4)_2$ were used as the laser gain materials for the hybrid SWCNT SA mode-locking experiments. The basic laser configuration was similar in all cases. Except for the $Tm:KLu(WO_4)_2$ laser, prism pairs were inserted in one of the cavity arms containing the output coupler for dispersion compensation. The lasers could be mode-locked either self-starting or by slightly moving a prism or the SWCNT-SA, without multiple pulsing in the broad power range starting from slightly above the lasing thresholds. Also for this hybrid type SWCNT-SA we did not observe any indication of damage or degradation of performance after several months of use at room temperature.

Figure 4 shows the measured autocorrelation traces of the mode-locked pulses from the four bulk solid-state lasers. The SWCNT-SA mode-locked $Yb:KLu(WO_4)_2$, Cr:forsterite and Cr:YAG lasers at ~1.07, ~1.24 and ~1.5 μm, respectively, generated nearly Fourier-limited pulses with pulse durations of 84–118 fs, whereas the $Tm:KLu(WO_4)_2$ laser delivered ~25 ps long pulses without dispersion compensation, see Table 1. The corresponding laser spectra are shown in the insets in Fig. 4. In stable mode-locked operation, output powers up to 62 mW were generated in $Yb:KLu(WO_4)_2$ with 1% output coupler (OC), 250 mW in Cr:forsterite with 7% OC, 85 mW in Cr:YAG with 2% OC and 167 mW in $Tm:KLu(WO_4)_2$ with 1.5% OC. In all cases, the recorded radio frequency spectra at the fundamental beat note of the laser repetition rates exhibited extinction ratios of > 55 dB above carrier. This is an evidence for stable cw single-pulse mode-locking without *Q*-switching instabilities.

4. Conclusions

As an important conclusion from our studies of SWCNT based SAs, we pinpoint the bundling topology of the nanotubes as the key parameter for the performance of the ultrabroadband SA device. Exploiting beneficial tube-to-tube interactions the absorber response can be accelerated without compromising low scattering losses. The independent consequences of curl and bundling allow combining apparently conflictive device properties such as low nonsaturable loss, nearly instantaneous switching speed, optical bandwidth, and low saturation fluence. The resulting device properties can be barely matched by existing semiconductor technology.

Careful control of the SWCNT bundling and curl in an optimised SA manufacturing process enabled the fabrication of one single device providing extremely broad (> 500 nm) ultrafast saturable absorption as well as hybrid devices with octave spanning absorption coverage. Thus, mode-locking of different bulk solid-state lasers in an almost 1000 nm wide spectral range (from ~1 to ~2 μm) could be achieved with one and the same transmission type SWCNT-SA. Further optimization of nanotube bundling, nonsaturable losses and absorption behaviour would make this SA device an attractive alternative to multiple saturable absorbers such as conventional SESAMs which in addition are difficult to fabricate for some of the above wavelengths.

Acknowledgements. We acknowledge financial support from the National Research Foundation (NRF) funded by the Korea Government (MEST) (Grant Nos 2011-0017494 and 2011-0001054).

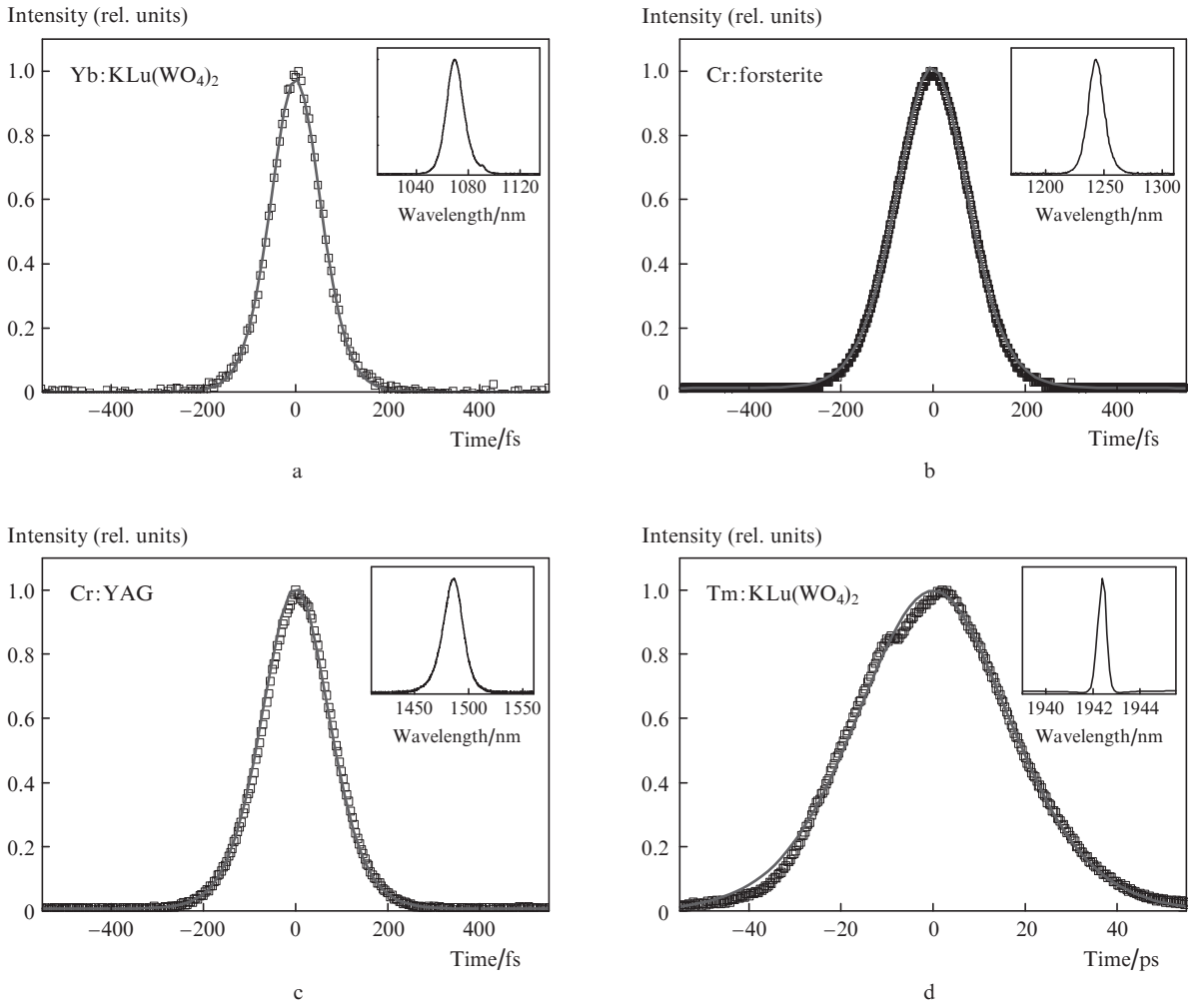

Figure 4. Autocorrelation traces of (a) Yb:$KLu(WO_4)_2$ (central wavelength, 1069 nm; pulse duration, $\tau = 84$ fs), (b) Cr:forsterite (1243 nm, 118 fs), (c) Cr:YAG (1485 nm, 113 fs), and (d) Tm:$KLu(WO_4)_2$ lasers (1942 nm, 25.4 ps), mode-locked with the same ultra-broadband hybrid type SWCNT-SA. Insets show the corresponding optical spectra [FWHM $\Delta\lambda = 15.4$ nm, $\tau\Delta\nu = 0.34$ (a), 15.6 nm, 0.36 (b), 21.3 nm, 0.33 (c), and 0.45 nm, 0.91 (d)]. The pulse duration τ (FWHM) is estimated assuming sech^2 intensity profiles.

References

1. Set S.Y., Yaguchi H., Tanaka Y., Jablonski M. *J. Lightwave Technol.*, **22**, 51 (2004).
2. Wang F., Rozhin A.G., Scardaci V., Sun Z., Hennrich F., White I.H., Milne W.I., Ferrari A.C. *Nature Nanotechnol.*, **3**, 738 (2008).
3. Hasan T., Sun Z., Wang F., Bonaccorso F., Tan P.H., Rozhin A.G., Ferrari A.C. *Adv. Mater.*, **21**, 3874 (2009).
4. Schibli T.R., Minoshima K., Kataura H., Itoga E., Minami N., Kazaoui S., Miyashita K., Tokumoto M., Sakakibara Y. *Opt. Express*, **13**, 8025 (2005).
5. Fong K.H., Kikuchi K., Goh C.S., Set S.Y., Grange R., Haiml M., Schlatter A., Keller U. *Opt. Lett.*, **32**, 38 (2007).
6. Yim J.H., Cho W.B., Lee S., Ahn Y.H., Kim K., Lim H., Steinmeyer G., Petrov V., Griebner U., Rotermund F. *Appl. Phys. Lett.*, **93**, 161106 (2008).
7. Cho W.B., Yim J.H., Choi S.Y., Lee S., Schmidt A., Steinmeyer G., Griebner U., Petrov V., Yeom D.-I., Kim K., Rotermund F. *Adv. Funct. Mater.*, **20**, 1937 (2010).
8. Khudyakov D.V., Lobach A.S., Nadtochenko V.A. *Opt. Lett.*, **35**, 2675 (2010).
9. Baek I.H., Choi S.Y., Lee H.W., Cho W.B., Petrov V., Agnesi A., Pasiskevicius V., Yeom D.-I., Kim K., Rotermund F. *Opt. Express*, **19**, 7833 (2011).
10. Schmidt A., Rivier S., Cho W.B., Yim J.H., Choi S.Y., Lee S., Rotermund F., Rytz D., Steinmeyer G., Petrov V., Griebner U. *Opt. Express*, **17**, 20109 (2009).
11. Schmidt A., Rivier S., Steinmeyer G., Yim J.H., Cho W.B., Lee S., Rotermund F., Pujol M.C., Mateos X., Aguilo M., Diaz F., Petrov V., Griebner U. *Opt. Lett.*, **33**, 729 (2008).
12. Agnesi A., Carrà L., Pirzio F., Reali G., Toncelli A., Tonelli M., Choi S.Y., Rotermund F., Griebner U., Petrov V. *J. Opt. Soc. Am. B*, **27**, 2739 (2010).
13. Agnesi A., Greborio A., Pirzio F., Ugolotti E., Reali G., Choi S.Y., Rotermund F., Griebner U., Petrov V. *IEEE J. Sel. Top. Quantum Electron.*, **18**, 74 (2012).
14. Chen H.-R., Wang Y.-G., Tsai C.-Y., Lin K.-H., Chang T.-Y., Tang J., Hsieh W.-F. *Opt. Lett.*, **36**, 1284 (2011).
15. Yang K., Zhao S., Zhang G., Cheng K., Zhao B., Xu J., He J., Wang Y. *Opt. Commun.*, **285**, 158 (2012).
16. Tan W.D., Chen F., Knize R.J., Zhang J., Tang D., Li L.-J. *Opt. Mater.*, **33**, 679 (2011).
17. Agnesi A., Greborio A., Pirzio F., Reali G., Choi S.Y., Rotermund F., Griebner U., Petrov V. *Appl. Phys. Express*, **3**, 112702 (2010).
18. Cho W.B., Yim J.H., Choi S.Y., Lee S., Griebner U., Petrov V., Rotermund F. *Opt. Lett.*, **33**, 2449 (2008).

19. Cho W.B., Choi S.-Y., Kim J.-W., Yeom D.-I., Kim K.-H., Rotermund F., Lim H.-J. *J. Opt. Soc. Korea*, **15**, 56 (2011).
20. Iliev H., Buchvarov I., Choi S.Y., Kim K., Rotermund F., Griebner U., Petrov V. *Appl. Phys. B*, **106**, 1 (2012).
21. Cho W.B., Schmidt A., Choi S.Y., Petrov V., Griebner U., Steinmeyer G., Lee S., Yeom D.-I., Rotermund F. *Opt. Lett.*, **35**, 2669 (2010).
22. Cho W.B., Schmidt A., Yim J.H., Choi S.Y., Lee S., Rotermund F., Griebner U., Steinmeyer G., Petrov V., Mateos X., Pujol M.C., Carvajal J.J., Aguiló M., Díaz F. *Opt. Express*, **17**, 11007 (2009).
23. Choi S.Y., Cho W.B., Yeom D.-I., Kim K., Rotermund F., Kim J.-H., Yee K.-J., Schmidt A., Steinmeyer G., Petrov V., Griebner U. *Techn. Digest Advanced Solid-State Photonics* (Istanbul, Turkey, 2011) paper AWB4.